AGU PUBLICATIONS

Geophysical Research Letters

RESEARCH LETTER
10.1002/2014GL061401

Key Points:
- Mariner 10 flyby magnetic field data are reanalyzed with MESSENGER techniques
- No secular variation in Mercury's dipole moment or dipole offset is evident
- Result constrains the low-degree power spectrum of Mercury's secular variation

Supporting Information:
- Data Set Description
- Table S1

Correspondence to:
L. C. Philpott,
lphilpott@eos.ubc.ca

Citation:
Philpott, L. C., C. L. Johnson, R. M. Winslow, B. J. Anderson, H. Korth, M. E. Purucker, and S. C. Solomon (2014), Constraints on the secular variation of Mercury's magnetic field from the combined analysis of MESSENGER and Mariner 10 data, *Geophys. Res. Lett.*, *41*, 6627–6634, doi:10.1002/2014GL061401.

Received 1 AUG 2014
Accepted 4 SEP 2014
Accepted article online 8 SEP 2014
Published online 3 OCT 2014

Constraints on the secular variation of Mercury's magnetic field from the combined analysis of MESSENGER and Mariner 10 data

Lydia C. Philpott[1], Catherine L. Johnson[1,2], Reka M. Winslow[1], Brian J. Anderson[3], Haje Korth[3], Michael E. Purucker[4], and Sean C. Solomon[5,6]

[1]Department of Earth, Ocean and Atmospheric Sciences, University of British Columbia, Vancouver, British Columbia, Canada, [2]Planetary Science Institute, Tucson, Arizona, USA, [3]The Johns Hopkins University Applied Physics Laboratory, Laurel, Maryland, USA, [4]NASA Goddard Space Flight Center, Greenbelt, Maryland, USA, [5]Department of Terrestrial Magnetism, Carnegie Institution of Washington, Washington, District of Columbia, USA, [6]Lamont-Doherty Earth Observatory, Columbia University, Palisades, New York, USA

Abstract Observations of Mercury's internal magnetic field from the Magnetometer on the MErcury Surface, Space ENvironment, GEochemistry, and Ranging (MESSENGER) spacecraft have revealed a dipole moment of 190 nT R_M^3 offset about 480 km northward from the planetary equator, where R_M is Mercury's radius. We have reanalyzed magnetic field observations acquired by the Mariner 10 spacecraft during its third flyby of Mercury (M10-III) in 1975 to constrain the secular variation in the internal field over the past 40 years. With the application of techniques developed in the analysis of MESSENGER data, we find that the dipole moment that best fits the M10-III data is 188 nT R_M^3 offset 475 km northward from the equator. Our results are consistent with no secular variation, although variations of up to 10%, 16%, and 35%, respectively, are permitted in the zonal coefficients g_1^0, g_2^0, and g_3^0 in a spherical harmonic expansion of the internal field.

1. Introduction

Magnetic field data acquired by the Mariner 10 spacecraft during its first flyby of Mercury in March 1974 [*Ness et al*., 1974] suggested that Mercury has a terrestrial-like magnetosphere with a weak intrinsic magnetic field. However, a definitive assessment of the geometry and origin of the internal field was not possible because of the equatorial spacecraft trajectory, the large distance of closest approach, and the substantial field variability on the outbound portion of the flyby [*Ness et al*., 1974].

Although the second Mariner 10 flyby of Mercury was too distant from the planet to measure the internal field, the third Mariner 10 flyby (hereafter M10-III) on 16 March 1975 confirmed the existence of an intrinsic magnetic field. The M10-III flyby had a closest approach distance of 327 km at geographic latitude 68°N, and analyses of the magnetic field data yielded a dipole moment of (136–350) nT R_M^3, where R_M is Mercury's radius (2440 km) and where the range of estimates reflected uncertainties in the external fields and the nondipole components of the internal field [*Ness et al*., 1975; *Connerney and Ness*, 1988]. Several hypotheses for the origin of Mercury's field were suggested, including a core dynamo field [e.g., *Connerney and Ness*, 1988] and remanent crustal fields [e.g., *Stephenson*, 1976; *Aharonson et al*., 2004].

More than three decades later, the Magnetometer on the MErcury Surface, Space ENvironment, GEochemistry, and Ranging (MESSENGER) spacecraft has provided measurements of Mercury's magnetic field environment during flybys in 2008 and 2009 and from orbit around the planet since March 2011. The flyby data confirmed the dominantly dipolar geometry of the internal field and indicated a core dynamo origin for the field [*Anderson et al*., 2008; *Purucker et al*., 2009; *Uno et al*., 2009]. Orbital data have enabled the development of a time-averaged model for Mercury's magnetic field. The model includes an average dipole moment of 190 nT R_M^3 offset 0.2 R_M northward from the planetary equator [*Anderson et al*., 2011, 2012; *Johnson et al*., 2012] and aligned with the planetary rotation axis.

Mercury's weak dipole moment, the northward offset of the magnetic equator from the planetary equator, and the axisymmetry of the field about the rotation axis yield a spherical harmonic description for the internal field dominated by the axial dipole term, g_1^0, but with important contributions from zonal harmonics of the next three highest degrees, g_2^0, g_3^0, and g_4^0 [*Anderson et al*., 2012]. This last result arises because the

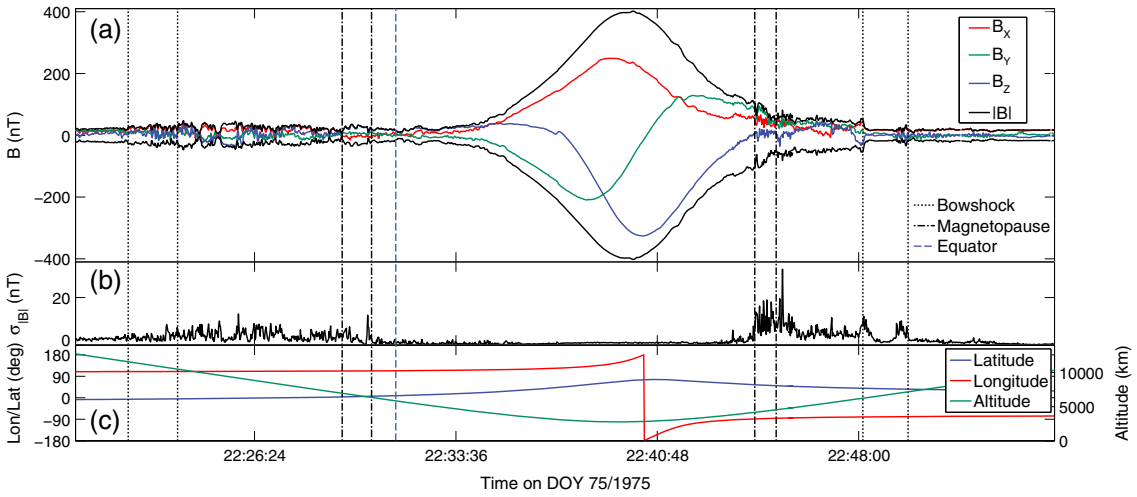

Figure 1. M10-III data in MSO coordinates. (a) Magnetic field components and magnitude averaged over 1.2 s intervals; crossing times for the magnetopause, bow shock, and magnetic equator are indicated by vertical lines. (b) Standard deviation in total magnetic field, $\sigma_{|\mathbf{B}|}$, over the averaging interval and spacecraft position in MSO coordinates and altitude. The magnetopause and inner and outer bow shock crossings for each boundary were identified by the methodology of *Winslow et al.* [2013], using the vector field, **B**, and $\sigma_{|\mathbf{B}|}$. DOY is day of the year.

spherical harmonic expansion for an offset dipole includes not only dipole and quadrupole (g_2^0) terms [*Bartels*, 1936] but higher-degree terms as well. The low-degree zonal terms provide first-order constraints on dynamo models for field generation in Mercury. Models proposed for weak dipole-dominated internal fields invoke aspects of the geometry of the fluid outer core, the presence of one or more stably stratified layers in the outer core, or feedback between the magnetospheric and core fields [*Stanley and Glatzmaier*, 2010]. Current dynamo modeling efforts are focused on capturing the asymmetry in the field about the geographic equator [e.g., *Cao et al.*, 2014].

The separation of nearly 40 years between the Mariner 10 and MESSENGER observations provides an opportunity to examine temporal variability (secular variation) in Mercury's internal magnetic field. Secular variation, and in particular the spatial power spectrum of secular variation, provides an additional important constraint on core dynamo models. For example, models that invoke a stably stratified layer at the top of the core to produce a weak field at and above the planetary surface also predict suppressed secular variation relative to models with no such layer [e.g., *Christensen*, 2006]. In this paper, we reanalyze the Mariner 10 and MESSENGER flyby data using techniques developed for the analysis of MESSENGER orbital data and search for evidence of secular variation in the planetary field. Given the limitations of the magnetic field data from the first Mariner 10 flyby, we consider data only from the third flyby. We first identify the instantaneous position of the magnetic equator in the M10-III data and compare this position to the range of values seen in the MESSENGER orbital data. We then use the magnetospheric model of *Johnson et al.* [2012] to examine any changes in the dipole moment or dipole offset. Finally, we briefly revisit the first two MESSENGER flybys. Taken together, the Mariner 10 and MESSENGER mission data sets constrain estimates of secular variation in the axial dipole, quadrupole, and octupole components of Mercury's dynamo field.

2. Analysis of M10-III Magnetic Field Data: Identification of Magnetospheric Boundaries and the Magnetic Equator

On its third flyby of Mercury, Mariner 10 entered the magnetosphere in the near-tail region and passed over the planet with a closest approach at an altitude of approximately 0.14 R_M before exiting the magnetosphere near dawn (Figure 1). We used 1.2 s averages of the magnetic field measurements (together with the standard deviation evaluated over 1.2 s) taken from *Lepping et al.* [1979] and the Planetary Data System to identify inner and outer limits for the bow shock and magnetopause boundary crossings following the method used for MESSENGER orbital data [*Winslow et al.*, 2013]. The resulting crossing times agree well with values given by *Ness et al.* [1976] and *Lepping et al.* [1979] and are shown in Figure 1.

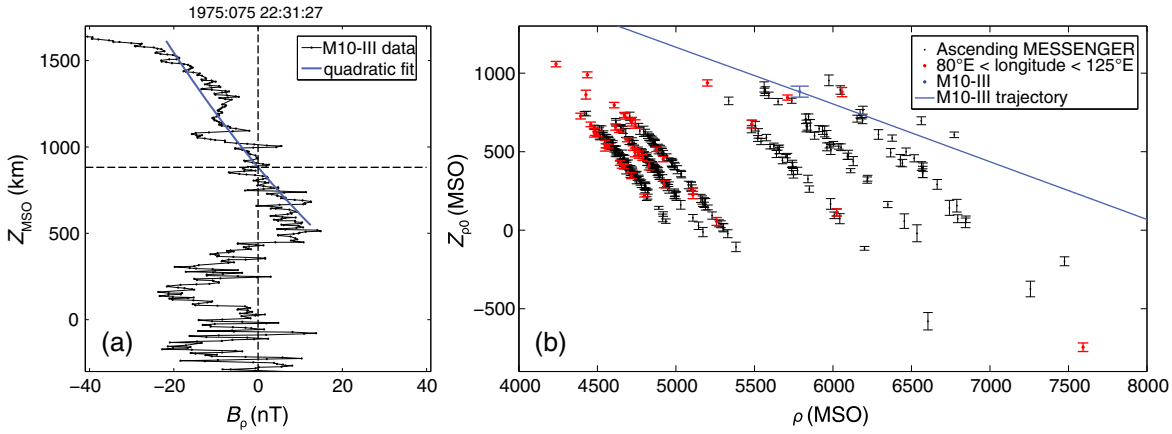

Figure 2. (a) Z_{MSO} versus B_ρ for M10-III near the magnetic equator crossing along with the quadratic function fit to the near-crossing data (solid blue line). The instantaneous equator crossing obtained from the fit is indicated by the dashed lines. The data shown here span the time interval 22:26–22:35 UTC on 16 March 1975. (b) Magnetic equator crossing $Z_{\rho 0}$ versus $\rho = (X^2_{MSO} + Y^2_{MSO})^{1/2}$ for M10-III (blue symbol and trajectory) and for the ascending legs of MESSENGER orbits (black symbols) between 24 March 2011 and 15 December 2012. MESSENGER magnetic equator crossings with MSO longitudes similar to that of the M10-III crossing (in the range 80°E to 125°E) are shown in red. Error bars indicate three standard errors.

The northward offset of Mercury's internal dipole field has been identified by the position of the magnetic equator in the MESSENGER orbital magnetic field data [*Anderson et al.*, 2011, 2012]. The geometry of MESSENGER's orbit around Mercury results in covariance among terms of even and odd degree in a spherical harmonic expansion for the internal field, similar to the covariance structure for M10-III [*Connerney and Ness*, 1988; *Korth et al.*, 2004]. Identification of the magnetic equator resolves this fundamental trade-off between the dipole and quadrupole terms. In Mercury solar orbital (MSO) coordinates (in which X_{MSO} is sunward, Z_{MSO} is northward and aligned with the planetary spin axis, and Y_{MSO} completes the right-handed system), the instantaneous location of the magnetic equator is given by the Z_{MSO} position at which $B_\rho = 0$, where B_ρ is the radial component of the magnetic field in MSO cylindrical coordinates. MESSENGER crossings of the magnetic equator between 24 March 2011 and 2 March 2012 yielded an average northward offset from the geographic equator of 479 ± 6 km for descending (low-altitude) crossings and 486 ± 74 km for ascending (high-altitude) crossings [*Anderson et al.*, 2012].

Following the same procedure, we identified the equator crossing region in the M10-III data. The spacecraft Z_{MSO} position as a function of B_ρ was fit by a quadratic function, and the instantaneous magnetic equator position, $Z_{\rho 0}$, was estimated by the $B_\rho = 0$ intercept of the fit (Figure 2a). The M10-III data yielded an equator offset of $Z_{\rho 0} = 882 \pm 35$ km, where the uncertainty estimate is three standard errors in the intercept of the quadratic fit.

The instantaneous equator position in the M10-III data is significantly northward of the average calculated from the MESSENGER orbital data. The M10-III equator crossing occurs at an altitude of 3415 km and an MSO longitude of 113°E, comparable to some of the high-altitude MESSENGER crossings. For comparison, we analyzed magnetic equator crossings identified at high altitudes on ascending legs of MESSENGER orbits between 24 March 2011 and 15 December 2012 at MSO longitudes ranging from 80°E to 125°E (Figure 2b). These crossings lie between 746 km south of the planetary equator and 1058 km north of the planetary equator. The M10-III equator offset falls within this range and is thus not atypical of instantaneous crossings from MESSENGER orbits with trajectories most similar to that of the M10-III flyby trajectory. The large variation in the MESSENGER crossings, particularly in the far tail, has been suggested to reflect tilting of the tail in response to north-south excursions in the solar wind velocity [*Anderson et al.*, 2012]. In addition, the M10-III equator crossing occurred within 1 min of the inbound inner magnetopause crossing and may therefore have been distorted by the near field of magnetopause currents.

3. Estimation of Dipole Moment

The time-averaged model for Mercury's magnetosphere developed by *Johnson et al.* [2012] was derived from MESSENGER orbital data between 24 March 2011 and 12 December 2011 and used the paraboloid

Table 1. Paraboloid Model Parameters From Fits to the M10-III, M1 and M2, and MESSENGER Orbital Data

Data Set	Z_d (km)	R_{SS} (R_M)	m (nT R_M^3)	RMS Misfit (nT)
M10-III (1975)	475 (best fit)	1.21	188	9.55
M1 and M2 (2008)	479	1.44 (M1), 1.38 (M2)	188	13.47
MESSENGER orbital data (2011) [*Johnson et al.*, 2012]	479	1.45	190	-

formulation for the magnetopause [*Alexeev et al.*, 2008, 2010]. A traditional spherical harmonic approach to coestimating internal and external fields was not used because of the trade-offs mentioned earlier and because MESSENGER magnetic field measurements are not taken in a source-free region [see *Johnson et al.*, 2012, and references therein]. The geometry of the MESSENGER orbit allowed all but one of the model parameters, discussed below, to be estimated directly from the data. A grid search for the final parameter, the dipole moment m, gave a value of $m = 190$ nT R_M^3.

3.1. Third Mariner 10 Flyby

To look for evidence of secular variation in Mercury's large-scale internal magnetic field, in particular in the dipole moment and its offset, or equivalently the low-degree zonal spherical harmonic terms, we compared paraboloid magnetospheric models fit to the M10-III data with the MESSENGER-derived model. As the instantaneous magnetic equator crossing observed during M10-III is not necessarily a good indication of the average dipole offset in 1975, we conducted a grid search over both the dipole offset, Z_d, and the dipole moment, m, to find the internal field model that best fits the data. The remaining magnetospheric model parameters were estimated as follows. The M10-III trajectory did not pass through the tail lobes or the tail current sheet, so it was not possible to estimate tail field parameters from this data set. However, along the M10-III trajectory, tail field contributions to the measured magnetic field were minimal, and we therefore set the tail parameters in the model to the MESSENGER average values. We estimated the magnetopause subsolar standoff distance, R_{SS}, from the dipole origin, for a given dipole offset, Z_d, from the observed magnetopause crossing positions during M10-III, given a model magnetopause [*Shue et al.*, 1997; *Winslow et al.*, 2013] corrected for solar wind aberration [*Johnson et al.*, 2012]. We used the dayside magnetopause crossings on the basis that these are more likely to provide a reliable estimate of R_{SS} than the nightside crossings. The sensitivity of our results to the choice of R_{SS} is discussed further below. Finally, MESSENGER magnetic equator observations have constrained the current tilt of the dipole moment from the spin axis to be less than 0.8° [*Anderson et al.*, 2012], and we set the dipole tilt, Ψ, to be zero in our grid searches. We return to the question of a possible nonzero tilt in the discussion.

In our grid search over Z_d and m, the best fit model was found by minimizing the root-mean-square (RMS) misfit in the field magnitude between the model and the M10-III data. We used step sizes of 1 nT R_M^3 in m and 50 km in Z_d, further refined to 25 km in the neighborhood of the initial minimum in RMS misfit.

The best fit model to the data has an RMS misfit of 9.6 nT, a dipole offset of $Z_d = 475$ km, and a dipole moment of $m = 188$ nT R_M^3 (Table 1). As previously reported [*Connerney and Ness*, 1988; *Korth et al.*, 2004], the M10-III trajectory results in a trade-off between the dipole offset and dipole moment. For example, a 25% increase in RMS misfit corresponds to a change in the (m, Z_d) parameters from (173 nT R_M^3, 560 km) to (206 nT R_M^3, 370 km) (indicated by blue triangles on Figure 3a). For a given dipole offset, the misfit minimum is better defined (indicated by black triangles on Figure 3a). For $Z_d = 475$ km, a 25% increase in RMS misfit corresponds to a range of dipole moments of (181–194) nT R_M^3.

The best fit model and the M10-III data are shown in Figure 3b. Also shown is the model with a dipole offset given by the observed instantaneous equator crossing position, $Z_d = 882$ km, and the corresponding best fit dipole moment $m = 123$ nT R_M^3. Although the latter model matches the data close to the magnetopause, it is clearly not a good fit to the observed planetary field inside the entire magnetosphere.

The magnetopause standoff distance, R_{SS}, can vary substantially over time scales of minutes [*Winslow et al.*, 2013]. The average outbound (dayside) magnetopause crossing yields an R_{SS} of 1.21 R_M. A similar calculation using the average inbound (nightside) crossing gives an R_{SS} of 1.40 R_M. This difference in R_{SS} values for the inbound and outbound crossings is not atypical of MESSENGER orbital observations. On time scales of

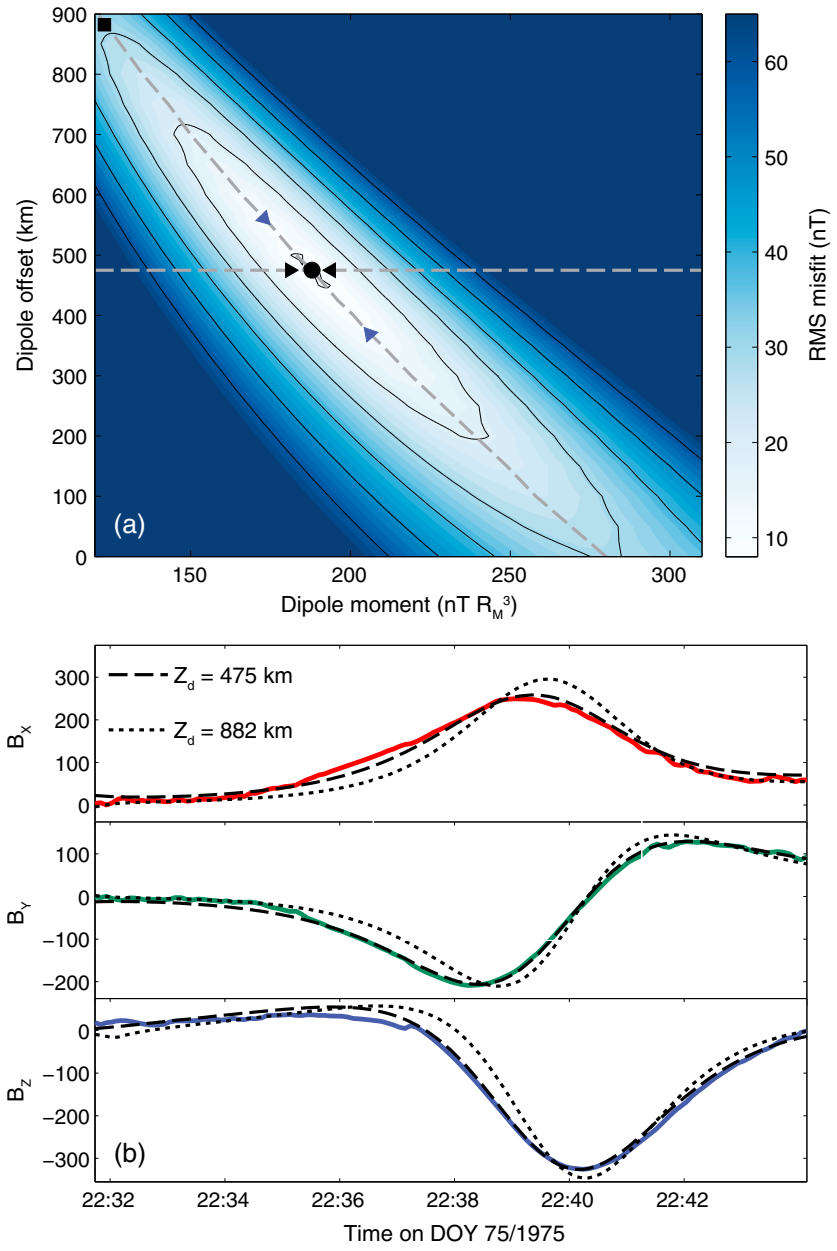

Figure 3. (a) RMS misfit between model and M10-III data obtained from a grid search over dipole moment and offset of the dipole from the geographic equator. Contours indicate misfits from 10 nT to 60 nT in 10 nT steps. The parameter pairs for the best fit offset of $Z_d = 475$ km and the M10-III magnetic equator offset of 882 km are marked by the filled black circle and filled square, respectively. The diagonal dashed line shows the trade-off between best fit dipole offset and dipole moment; blue triangles correspond to parameter pairs that yield an RMS misfit 25% above the minimum value. The horizontal dashed line shows the location of an RMS misfit profile corresponding to the best fit dipole offset; a 25% increase above the minimum misfit would yield dipole moments shown by the black triangles. (b) Magnetic field observations from M10-III inside the magnetopause (solid lines) and best fit models to the data for dipole offsets of 475 km (dashed line) and 882 km (dotted line).

Mercury's orbital period, R_{SS} also varies with Mercury's heliocentric distance, r_{helio} [*Korth et al.*, 2012; *Johnson et al.*, 2013]. MESSENGER orbital observations indicate an average relation of the form $R_{SS} = 1.99\ (r_{helio})^{1/3}$. This relation yields an R_{SS} value of 1.54 R_M, given a heliocentric distance of 0.356 AU at the time of the M10-III flyby.

We assessed the impact of our choice of R_{SS} on our estimate of dipole moment as follows: for each of the R_{SS} values of 1.40 R_M and 1.54 R_M, we held the dipole offset constant at the best fit value of 475 km obtained above, and we found a best fit dipole moment by minimizing the misfit between the magnetospheric model

and the M10-III data. The resulting best fit dipole moment was insensitive to the choice of R_{SS}, varying by only 2 nT R_M^3 from the value obtained using the initial R_{SS} estimate of 1.21 R_M.

3.2. MESSENGER Flybys

We reanalyzed the first two MESSENGER flybys of Mercury (hereafter M1 and M2, respectively) on 14 January and 6 October 2008 to investigate whether the magnetic field measured during those flybys is consistent with the time-averaged magnetospheric model determined from MESSENGER orbital data [*Johnson et al.*, 2012]. The negligible latitudinal variations during the M1 and M2 equatorial trajectories meant that it was not possible to identify a magnetic equator crossing from data acquired during either flyby.

We set all parameters in the model to the time-averaged values except the magnetopause standoff distance, R_{SS}, and the dipole moment, m. Magnetopause crossing positions were taken from *Anderson et al.* [2008] and *Slavin et al.* [2009] for M1 and M2, respectively. For both flybys the R_{SS} estimates from the R_{SS}—r_{helio} relation were found to be very similar to the R_{SS} value calculated from the outbound (dayside) magnetopause crossing position. The corresponding grid searches over dipole moment also gave similar results, so we consider the outbound R_{SS} values and the associated dipole moment searches to best represent the flyby data (Table 1). The best fit dipole moment of 188 nT R_M^3 for the combined M1 and M2 data is consistent with the time-averaged magnetospheric model of *Johnson et al.* [2012].

4. Discussion and Conclusions

Magnetic field observations from the third Mariner 10 flyby and the MESSENGER flybys of Mercury have been analyzed using approaches applied to the MESSENGER orbital data to investigate changes in the dipole moment and offset over the intervening four decades. The magnetic field measured along the M10-III trajectory was dominated by contributions from the magnetopause and the internal dipole field. Paraboloid magnetospheric models were generated in which the magnetopause fields were prescribed using $R_{SS} = 1.21$ R_M, and a grid search was conducted over dipole moment, m, and dipole offset from the geographic equator, Z_d. The best fit model is indistinguishable from that of the MESSENGER orbital data (Table 1). The best fit value for the dipole offset yields a substantially lower misfit than that obtained using an offset given by the magnetic equator crossing indicated by the M10-III data. This result supports the conclusion that the instantaneous value is unlikely to be representative of the average dipole offset. The magnetic equator position indicated by the M10-III data, although farther north than the MESSENGER average, is well within the observed range in MESSENGER orbital data and likely an indication of a tilted current sheet or perhaps substantial magnetopause fields rather than a high offset of instantaneous magnetic equator. The first two MESSENGER flybys also yield best fit moments consistent with that obtained from MESSENGER orbital data.

Although the best fit models yield no resolvable evidence for secular variation in either the dipole moment or its offset, the trade-off between dipole moment and offset provides upper bounds on secular variation in the axisymmetric part of the field. We find that a 25% increase in RMS misfit results in a noticeably worse fit to the data, and we take the (m, Z_d) values of (206 nT R_M^3, 370 km) and (173 nT R_M^3, 560 km) corresponding to such a misfit as upper limits on secular variation. The equivalent spherical harmonic representation of this offset dipole field can be found with the relationships given in Table 3 of *Anderson et al.* [2012]. The above (m, Z_d) limits correspond to low-degree axial spherical harmonic coefficients g_1^0, g_2^0, and g_3^0 of (−206, −62, −14) nT and (−173, −79, −27) nT, respectively, and the mean values from the MESSENGER orbital data are (−190, −75, −22) nT [*Anderson et al.*, 2012]. Thus, changes in the dipole moment (or the g_1^0 coefficient) of less than 10% may be accompanied by changes in the degree 2 and degree 3 axial terms of up to 16% and 35%, respectively, yielding substantial changes in the slope of the low-degree spatial power spectrum. We did not consider the g_4^0 term here, as its value indicated by MESSENGER orbital data is small, $|g_4^0| < 6$ nT.

The results reported here were derived under the assumption that there is no contribution from nonaxisymmetric low-degree terms in the field. We verified that there is no substantial tilt of the dipole axis from the spin axis as follows. We subtracted the magnetopause and tail fields of the best fit model from the M10-III data sampled at 6 s intervals. On the assumption that the remaining signal is primarily that of an offset dipole, we calculated the apparent latitude and longitude of the pole from the magnetic field direction at each point along the trajectory. The pole latitude is measured on a sphere centered on the offset dipole ($Z_d = 475$ km). Pole positions at high altitudes were clearly affected by errors in the model estimate of the

magnetopause fields. For data acquired at altitudes less than 650 km, the pole positions cluster about a mean position of 87.9°N, 78.8° E. A magnetospheric model fit with a dipole tilt of 2.1° in the azimuth direction 78.8°E gave less than a 3% improvement (0.3 nT) in RMS misfit over the zero-tilt model. The 95% confidence limit on the pole position is 0.7° if all 42 estimates of the pole position at 6 s sampling are considered to be independent. However, larger confidence limits result if all of the observations are not taken to be independent. MESSENGER orbital data indicate an upper bound on the current dipole tilt of 0.8° via analysis of the magnetic equator crossings, and constraints on the tilt direction are poor [*Anderson et al*., 2012]. We conclude that there is no evidence of significant secular variation in Mercury's dipole tilt. Furthermore, we verified via fits to the paraboloid magnetospheric model that any dipole offset in the plane of the geographic equator is insignificant in comparison with the offset in the *Z* direction. Taken together, these results confirm that there has been no observable secular variation in the nonaxial contributions to the field at low spherical harmonic degree and order.

The presence of secular variation in Earth's magnetic field is well documented [e.g., *Finlay et al*., 2010]. Studies of the magnetic fields of Jupiter and Saturn have revealed no definitive secular variation in the internal field of either body over more than 30 years of observations [*Yu et al*., 2010; *Cao et al*., 2011; *Ridley*, 2012]. It is interesting to consider whether Earth-like secular variation would be detectable in the Mercury magnetic field data. Between 1975 and 2010, secular variation in the terrestrial axial dipole, g_1^0, axial quadrupole, g_2^0, and nonaxial dipole terms, g_1^1 and h_1^1, resulted in changes in these terms of 2%, 21%, 27%, and 15%, respectively [*Finlay et al*., 2010]. At Mercury, a 2% change in the dipole moment corresponds to a variation of less than 4 nT R_M^3, and Earth-like percentage variations in g_1^1 and h_1^1 would be difficult to assess via changes in the pole position, given the negligible tilt of the dipole moment from the spin axis. From our upper limits on changes in tilt and the low-degree axial terms at Mercury, Earth-like relative magnitudes of secular variation are permitted but not required by the M10-III data. From a dynamical standpoint, the spatial power spectrum of secular variation at Mercury may be quite different from that at Earth. Dynamo models that match the weak, equatorially asymmetric field with a stably stratified layer at the top of the core or through a combination of volumetric buoyancy and equatorially symmetric core-mantle heat flow have characteristic timescales for secular variation in the low-degree terms that are of order 1000 years, and the amplitude of the variations is small [*Christensen and Wicht*, 2008; *Cao et al*., 2014]. Strong secular variation in g_1^0 and g_2^0 (±100% of the peak values) occurs in oscillatory dynamos (e.g., *Dietrich and Wicht* [2013], though these models were not specifically adapted to Mercury), but the oscillatory time scale of a few thousand years results in very little change in these coefficients over the 40 year interval between the times of the third Mariner 10 flyby and MESSENGER orbital observations. Our results provide the first observational constraint on secular variation in Mercury's internal magnetic field at low spherical harmonic degree.

Acknowledgments

The Mariner 10 magnetic field data were obtained from the Planetary Data System (PDS). LCP, CLJ, and RMW acknowledge support from the Natural Sciences and Engineering Research Council of Canada. The MESSENGER project is supported by the NASA Discovery Program under contracts NAS5-97271 to The Johns Hopkins University Applied Physics Laboratory and NASW-00002 to the Carnegie Institution of Washington. CLJ acknowledges support from MESSENGER Participating Scientist grant NNX11AB84G. MESSENGER data are available from the PDS (https://pds.jpl.nasa.gov).

The Editor thanks two anonymous reviewers for their assistance in evaluating this paper.

References

Aharonson, O., M. T. Zuber, and S. C. Solomon (2004), Crustal remanence in an internally magnetized non-uniform shell: A possible source for Mercury's magnetic field, *Earth Planet. Sci. Lett.*, *218*, 261–268, doi:10.1016/S0012-821X(03)00682-4.

Alexeev, I. I., E. S. Belenkaya, S. Y. Bobrovnikov, J. A. Slavin, and M. Sarantos (2008), Paraboloid model of Mercury's magnetosphere, *J. Geophys. Res.*, *113*, A12210, doi:10.1029/2008JA013368.

Alexeev, I. I., et al. (2010), Mercury's magnetospheric magnetic field after the first two MESSENGER flybys, *Icarus*, *209*, 23–39, doi:10.1016/j.icarus.2010.01.024.

Anderson, B. J., M. H. Acuña, H. Korth, M. E. Purucker, C. L. Johnson, J. A. Slavin, S. C. Solomon, and R. L. McNutt Jr. (2008), The structure of Mercury's magnetic field from MESSENGER's first flyby, *Science*, *321*, 82–85, doi:10.1126/science.1159081.

Anderson, B. J., C. L. Johnson, H. Korth, M. E. Purucker, R. M. Winslow, J. A. Slavin, S. C. Solomon, R. L. McNutt Jr., J. M. Raines, and T. H. Zurbuchen (2011), The global magnetic field of Mercury from MESSENGER orbital observations, *Science*, *333*, 1859–1862, doi:10.1126/science.1211001.

Anderson, B. J., C. L. Johnson, H. Korth, R. M. Winslow, J. E. Borovsky, M. E. Purucker, J. A. Slavin, S. C. Solomon, M. T. Zuber, and R. L. McNutt Jr. (2012), Low-degree structure in Mercury's planetary magnetic field, *J. Geophys. Res.*, *117*, E00L12, doi:10.1029/2012JE004159.

Bartels, J. (1936), The eccentric dipole approximating the Earth's magnetic field, *J. Geophys. Res.*, *41*, 225–250, doi:10.1029/TE041i003p00225.

Cao, H., C. T. Russell, U. R. Christensen, M. K. Dougherty, and M. E. Burton (2011), Saturn's very axisymmetric magnetic field: No detectable secular variation or tilt, *Earth Planet. Sci. Lett.*, *304*, 22–28, doi:10.1016/j.epsl.2011.02.035.

Cao, H., J. M. Aurnou, J. Wicht, W. Dietrich, K. M. Soderlund, and C. T. Russell (2014), A dynamo explanation for Mercury's anomalous magnetic field, *Geophys. Res. Lett.*, *41*, 4127–4134, doi:10.1002/2014GL060196.

Christensen, U. R. (2006), A deep dynamo generating Mercury's magnetic field, *Nature*, *444*, 1056–1058, doi:10.1038/nature05342.

Christensen, U. R., and J. Wicht (2008), Models of magnetic field generation in partly stable planetary cores: Applications to Mercury and Saturn, *Icarus*, *196*, 16–34, doi:10.1016/j.icarus.2008.02.013.

Connerney, J. E. P., and N. F. Ness (1988), Mercury's magnetic field and interior, in *Mercury*, edited by F. Vilas, C. R. Chapman, and M. S. Matthews, pp. 494–513, Univ. of Ariz. Press, Tucson, Ariz.

Dietrich, W., and J. Wicht (2013), A hemispherical dynamo model: Implications for the Martian crustal magnetization, *Phys. Earth Planet. Inter.*, *217*, 10–21, doi:10.1016/j.pepi.2013.01.001.

Finlay, C. C., et al. (2010), International geomagnetic reference field: The eleventh generation, *Geophys. J. Int.*, *183*, 1216–1230, doi:10.1111/j.1365-246X.2010.04804.x.

Johnson, C. L., et al. (2012), MESSENGER observations of Mercury's magnetic field structure, *J. Geophys. Res.*, *117*, E00L14, doi:10.1029/2012JE004217.

Johnson, C. L., et al. (2013), Induced magnetic fields at Mercury from MESSENGER observations, *Lunar Planet. Sci.*, *44*, abstract 1311.

Korth, H., B. J. Anderson, M. H. Acuña, J. A. Slavin, N. A. Tsyganenko, S. C. Solomon, and R. L. McNutt Jr. (2004), Determination of the properties of Mercury's magnetic field by the MESSENGER mission, *Planet. Space Sci.*, *52*, 733–746, doi:10.1016/j.pss.2003.12.008.

Korth, H., B. J. Anderson, C. L. Johnson, R. M. Winslow, J. A. Slavin, M. E. Purucker, S. C. Solomon, and R. L. McNutt Jr. (2012), Characteristics of the plasma distribution in Mercury's equatorial magnetosphere derived from MESSENGER Magnetometer observations, *J. Geophys. Res.*, *117*, A00M07, doi:10.1029/2012JA018052.

Lepping, R. P., N. F. Ness, and K. W. Behannon (1979), Summary of Mariner 10 magnetic field and trajectory data for Mercury I and III encounters, NASA-TM 80600, NASA Goddard Space Flight Center, Greenbelt, Md.

Ness, N. F., K. W. Behannon, R. P. Lepping, Y. C. Whang, and K. H. Schatten (1974), Magnetic field observations near Mercury: Preliminary results from Mariner 10, *Science*, *185*, 151–160, doi:10.1126/science.185.4146.151.

Ness, N. F., K. W. Behannon, R. P. Lepping, and Y. C. Whang (1975), Magnetic field of Mercury confirmed, *Nature*, *255*, 204–205, doi:10.1038/255204a0.

Ness, N. F., K. W. Behannon, R. P. Lepping, and Y. C. Whang (1976), Observations of Mercury's magnetic field, *Icarus*, *28*, 479–488, doi:10.1016/0019-1035(76)90121-4.

Purucker, M. E., T. J. Sabaka, S. C. Solomon, B. J. Anderson, H. Korth, M. T. Zuber, and G. A. Neumann (2009), Mercury's internal magnetic field: Constraints on large- and small-scale fields of crustal origin, *Earth Planet. Sci. Lett.*, *285*, 340–346, doi:10.1016/j.epsl.2008.12.017.

Ridley, V. A. (2012), Jovimagnetic secular variation, PhD thesis, Univ. of Liverpool, Liverpool, U. K.

Shue, J.-H., J. K. Chao, H. C. Fu, C. T. Russell, P. Song, K. K. Khurana, and H. J. Singer (1997), A new functional form to study the solar wind control of the magnetopause size and shape, *J. Geophys. Res.*, *102*, 9497–9511, doi:10.1029/97JA00196.

Slavin, J. A., et al. (2009), MESSENGER observations of magnetic reconnection in Mercury's magnetosphere, *Science*, *324*, 606–610, doi:10.1126/science.1172011.

Stanley, S., and G. A. Glatzmaier (2010), Dynamo models for planets other than Earth, *Space Sci. Rev.*, *152*, 617–649, doi:10.1007/s11214-009-9573-y.

Stephenson, A. (1976), Crustal remanence and the magnetic moment of Mercury, *Earth Planet. Sci. Lett.*, *28*, 454–458, doi:10.1016/0012-821X(76)90206-5.

Uno, H., C. L. Johnson, B. J. Anderson, H. Korth, and S. C. Solomon (2009), Modeling Mercury's internal magnetic field with smooth inversions, *Earth Planet. Sci. Lett.*, *285*, 328–339, doi:10.1016/j.epsl.2009.02.032.

Winslow, R. M., B. J. Anderson, C. L. Johnson, J. A. Slavin, H. Korth, M. E. Purucker, D. N. Baker, and S. C. Solomon (2013), Mercury's magnetopause and bow shock from MESSENGER Magnetometer observations, *J. Geophys. Res. Space Physics*, *118*, 2213–2227, doi:10.1002/jgra.50237.

Yu, Z. J., H. K. Leinweber, and C. T. Russell (2010), Galileo constraints on the secular variation of the Jovian magnetic field, *J. Geophys. Res.*, *115*, E03002, doi:10.1029/2009JE003492.